CHEMISTRY OF MATERIALS

ARTICLE

pubs.acs.org/cm

Hierarchical Dendrite-Like Magnetic Materials of Fe_3O_4, γ-Fe_2O_3, and Fe with High Performance of Microwave Absorption

Genban Sun,*[,†] Bingxiang Dong,[†] Minhua Cao,*[,‡] Bingqing Wei,*[,§] and Changwen Hu[‡]

[†]College of Chemistry, Beijing Normal University, Beijing 100875, P. R. China

[‡]Key Laboratory of Cluster Science, Ministry of Education of China and Department of Chemistry, Beijing Institute of Technology, Beijing 100081, P. R. China

[§]Department of Mechanical Engineering, University of Delaware, Newark, Delaware 19716, United States

Supporting Information

ABSTRACT: Iron-based microstructured or nanostructured materials, including Fe, γ-Fe_2O_3, and Fe_3O_4, are highly desirable for magnetic applications because of their high magnetization and a wide range of magnetic anisotropy. An important application of these materials is use as an electromagnetic wave absorber to absorb radar waves in the centimeter wave (2−18 GHz). Dendrite-like microstructures were achieved with the phase transformation from dendritic α-Fe_2O_3 to Fe_3O_4, Fe by partial and full reduction, and γ-Fe_2O_3 by a reduction−oxidation process, while still preserving the dendritic morphology. The investigation of the magnetic properties and microwave absorbability reveals that the three hierarchical microstructures are typical ferromagnets and exhibit excellent microwave absorbability. In addition, this also confirms that the microwave absorption properties are ascribed to the dielectric loss for Fe and the combination of dielectric loss and magnetic loss for Fe_3O_4 and γ-Fe_2O_3.

KEYWORDS: dendrite-like, microstructure, magnetic materials, microwave-absorbing materials, nanostructure

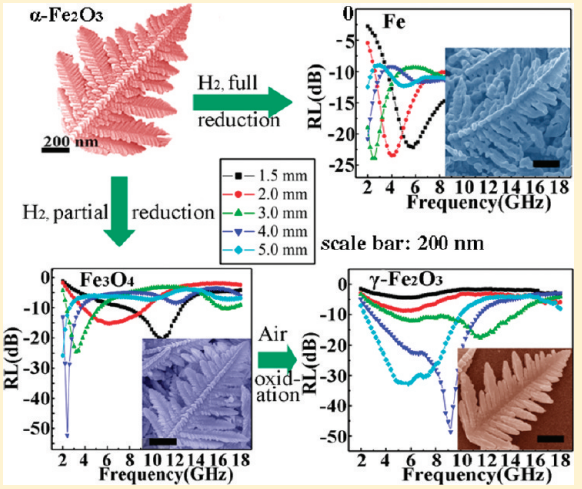

INTRODUCTION

In recent years, there is an intense interest in the hierarchical assembly of one-dimensional nanoscale building blocks into ordered superstructures or complex architectures because of their widespread potential applications in catalysis, drug delivery, acoustic insulation, photonic crystals, and other areas.[1] Moreover, the particular structural features of the hierarchical nanostructures have large surface areas and allow for heterostructures, which can be applied in photovoltaics and multifunctional nanoelectronics.[2] A dendrite is a kind of material that has a main stem from which many side branches grow out and a hierarchical structure with primary, secondary, tertiary, and even higher-order branches.[3] Because the single-crystal dendritic α-Fe_2O_3 has been successfully reported by our group,[4] many efforts have been focused on the preparation of various dendritic nanostructures or microstructures, including metals such as Ag, Cu, Co, and Ni,[5] alloys such as CuNi,[6] semiconductor transition metal chalcogenides such as ZnO, WO_3, CdS, Ag_2Se, PbTe, and so on.[7] Recently, branched bismuth telluride/sulfide nanorods were prepared by using a biomolecular surfactant by Ramanath et al.[8] However, among the prior research on the synthesis of the microstructured or nanostructured dendritic materials, to the best of our knowledge, no work has been reported on the synthesis of Fe, γ-Fe_2O_3, and Fe_3O_4 dendritic microstructures.

Magnetic nanomaterials have been the subject of increasing interest because of their physical properties and potential technological applications.[9] The magnetic properties of nanomaterials have been considered to be highly associated with their size, structure, cryastallinity, etc. Microwave absorbing materials with low reflection and high absorption based on the magnetic materials have received extensive attention because of their promising application in electronic devices in commerce, industry, and military affairs. For example, Ohkoshi and co-workers synthesized a new series of $Ga_xFe_{2-x}O_3$ ($0.10 \leq x \leq 0.67$) magnetic nanoparticles by the combination of reversemicelle and sol−gel techniques or only the sol−gel method and found that the magnetic properties are dependent on the amount of Ga dopant in ε-Fe_2O_3. What is more important is that these materials can absorb different electromagnetic waves in a wide range between 35 and 190 GHz on the basis of their different amounts of Ga dopant.[10] Recently, Fe nanoflakes, Fe_3O_4 nanospheres, ε-Fe_2O_3

Received: December 1, 2010
Revised: January 24, 2011
Published: February 15, 2011

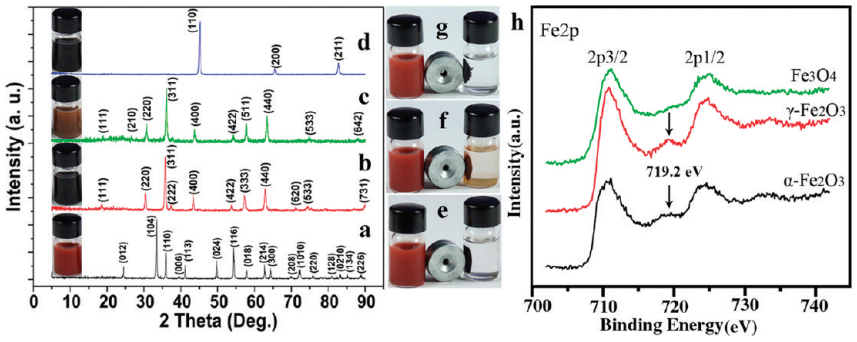

Figure 1. XRD patterns and photographs of the typical as-prepared samples. (a) α-Fe_2O_3, (b) Fe_3O_4, (c) γ-Fe_2O_3, and (d) Fe dendritic microstructures. Comparison photographs α-Fe_2O_3 dendritic microstructures with (e) Fe_3O_4, (f) γ-Fe_2O_3, and (g) Fe dendritic microstructures separated by a magnet. (h) Fe 2p core-level XPS spectra of the typical as-prepared samples.

nanomaterial and ε-$Al_xFe_{2-x}O_3$ nanomagnets ($0 \leq x \leq 0.40$) with a particle size between 25 and 50 nm with their application as electromagnetic wave absorber have been successfully reported.[11] Therefore, it is very valuable to study the relationship between their structure and morphology and the magnetic properties of nanomatetials, which could influence their applications as microwave absorbers. In addition, as is well-known, iron-based microstructured or nanostructured materials, including Fe, γ-Fe_2O_3, and Fe_3O_4, are highly desirable for magnetic applications because of their high magnetization and wide range of magnetic anisotropy.[12]

Dendritic micropines of α-Fe_2O_3 with single-crystal structures have been successfully synthesized by the hydrothermal reaction of $K_3[Fe(CN)_6]$ in aqueous solution at suitable temperatures in our group.[4] However, compared with other iron-based ferromagnetic materials, such as Fe_3O_4, γ-Fe_2O_3, and Fe, α-Fe_2O_3, they do not possess excellent magnetic properties because of containing only Fe in the +3 oxidation state and their antiferromagnetism.[13] The synthesis of reduced or other crystal-shaped iron oxides with dendritic microstructures or nanostructures, especially Fe_3O_4 (inverse spinel structure), γ-Fe_2O_3, and Fe, is acknowledged to be an important challenge. Hence, the idea comes of whether or not the α-Fe_2O_3 dendritic micropines could be converted to the above iron-based materials and still maintain the dendritic shape of the precursor. Inspired by this thought, we achieved the phase transformation from α-Fe_2O_3 to Fe_3O_4 and Fe by partial and full reduction and γ-Fe_2O_3 by a reduction−oxidation process, while still preserving the dendritic morphology (Experimental Section). To the best of our knowledge, this represents the first synthesis of the important dendritic ferromagnetic materials, Fe_3O_4, γ-Fe_2O_3, and Fe. Conversion of the α-Fe_2O_3 structure to Fe_3O_4 spinel involves a change from a hexagonal close-packed oxide ion array (α-Fe_2O_3) to a cubic close-packed array (Fe_3O_4). This is not a topotactic phase change. It involves sheaving of the oxide ion planes from AB to ABC stacking; yet this significant structural change can occur without destroying the dendritic morphology, including the conversion from Fe_3O_4 to γ-Fe_2O_3 and then to Fe. Preliminary magnetic characterization and the microwave absorption properties of Fe, γ-Fe_2O_3, and Fe_3O_4 dendritic microstructures are presented. In addition, the current electromagnetic materials only exhibit absorbing peaks at high frequency (12−18 GHz). It is still a challenge to obtain the materials that own strong microwave absorption in low (2−6 GHz) or middle (6−12 GHz) frequencies. Hence, it is valuable to explore a kind of microwave absorber that shows strong absorption in low or middle frequency during 2−18 GHz and investigate the relationship between the structure and electromagnetic properties.

EXPERIMENTAL SECTION

Synthesis. In a typical synthesis of Fe_3O_4, γ-Fe_2O_3, and Fe micropine dendrites, $K_3[Fe(CN)_6]$ was dissolved in distilled water to form a clear solution with a concentration of 0.1 mol/L, which was placed in a Teflon-sealed autoclave and maintained at a temperature of 140 °C for 2 d. The red product was isolated by centrifugation, repeatedly washed with distilled water and absolute ethanol, and dried at 50 °C in air. This procedure leads to dendritic micropines of α-Fe_2O_3 with a single-crystal structure as described in ref 4. Reduction for Fe micropine dendrites was achieved by heating at 350 °C for 1 h under a 20 mL/min H_2 atmosphere, and reduction for Fe_3O_4 micropine dendrites was achieved by heating at 350 °C for 1 h under a 10 mL/min H_2 and a 120 mL/min Ar atmosphere. For the preparation of γ-Fe_2O_3 micropine dendrites, the as-prepared Fe_3O_4 micropine dendrites were heated at 150 °C for 2 h in air.

Characterization. The composition and phase purity of the as-synthesized samples were analyzed by XRD with monochromatized Cu Kα (λ = 1.54178 Å) incident radiation by a Shimadzu XRD-6000 operated at 40 kV voltage and 50 mA current. XRD patterns were recorded from 5° to 90° (2θ) with a scanning step of 0.02°. The size distribution and morphologies of the samples were characterized by a JEOL JSM-6700F field-emission SEM. A JEOL JEM-2010F TEM operating at 200 kV accelerating voltage was used for TEM, HRTEM, and SAED analysis. X-ray photoelectron spectra (XPS) were recorded on a PHI-5300 ESCA spectrometer (Perkin-Elmer) to characterize the surface composition with the Al Kα line as the excitation source. Magnetization measurements of the typical samples were performed on a Quantum Design MPMS-XL5 SQUID magnetometer. Magnetic hysteresis loop measurements were performed at T = 5 and 300 K. The magnetic Fe, γ-Fe_2O_3, and Fe_3O_4 micropine dendrites/paraffin composite samples were prepared by uniformly mixing the micropines in a paraffin matrix and then pressing the mixture into a cylindrical shaped compact (Φ_{outer} = 7.00 mm and Φ_{inner} = 3.04 mm). The electromagnetic parameters of the microstructures or nanostructures composite samples with 70 wt % of the micropines were measured in the 2−18 GHz range by using an Agilent E8362B vector network analyzer.

RESULTS AND DISCUSSION

The phase composition and structure of the precursor α-Fe_2O_3 and the as-transformed samples were examined by powder X-ray diffraction (XRD). As shown in panel (a) of Figure 1, the precursor is pure α-Fe_2O_3 phase (hematite), which has a rhombohedral structure with lattice parameters of a = 0.504 and c = 1.375 nm. The XRD patterns of the three samples after phase transformation are shown in panels (b)−(d) of Figure 1. The sharp reflections of the XRD pattern of iron (Figure 1d) can be attributed to the body-centered cubic phase of Fe

dx.doi.org/10.1021/cm103441u |*Chem. Mater.* 2011, 23, 1587–1593

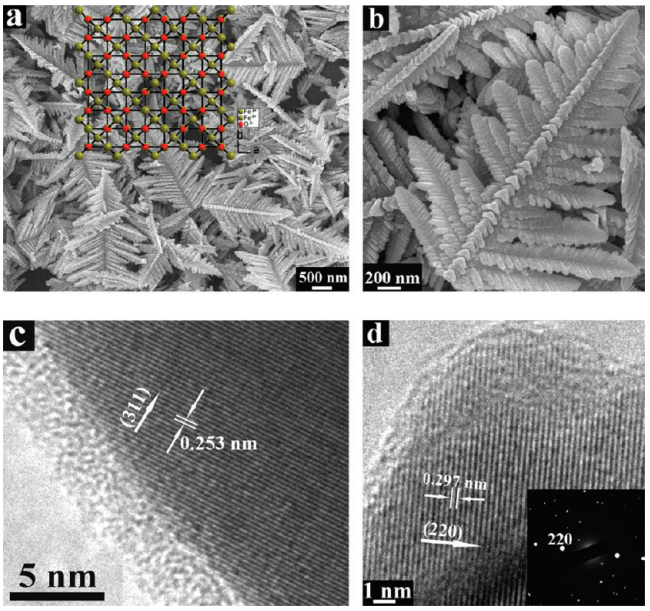

Figure 2. (a, b) SEM, (c, d) HRTEM images of Fe_3O_4 dendritic microstructures. Inset of panels (a) and (d) are the crystal structure of Fe_3O_4 and the SAED pattern, respectively.

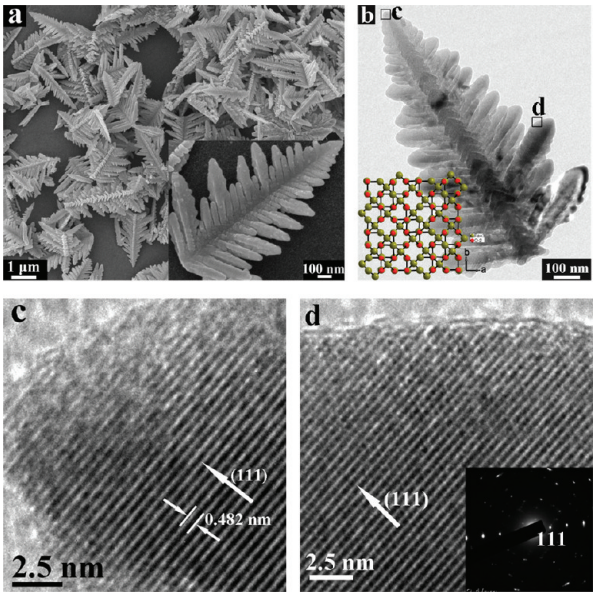

Figure 3. (a) SEM, (b) TEM, (c, d) HRTEM images of γ-Fe_2O_3 dendritic microstructures. The insets of panels (a) and (d) are magnified SEM images of a single dendrite and the SAED pattern. Inset of panel (b) is the crystal structure of γ-Fe_2O_3.

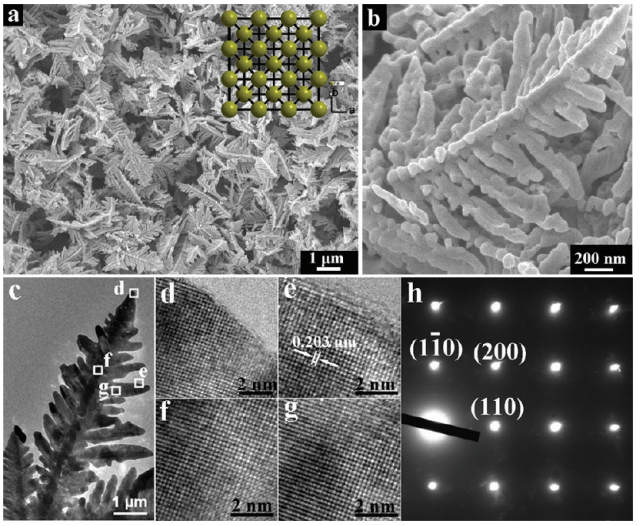

Figure 4. (a, b) SEM, (c) TEM images of Fe dendritic microstructures, (d−g) HRTEM images taken at different regions as marked in (c). (h) Typical SAED pattern of iron dendrite microstructures. Inset of panel (a) is the crystal structure of γ-Fe_2O_3 of Fe.

(JCPDS card 87-0721), without indication of the precursor or other crystalline byproducts. The patterns of panels (b) and (c) of Figure 1 are almost same, matching both the magnetite Fe_3O_4 (JCPDS card 87-0245) and the maghemite γ-Fe_2O_3 (JCPDS card 39-1346). The XRD patterns of magnetite and maghemite just differ in a few low intensity reflections (<5%) present at 2θ = 23.8° and 26.1°. Therefore, X-ray photoelectron spectrum (XPS) measurements (Figure 1h) have to be consulted to unambiguously assign the crystal phase because XPS is very sensitive to Fe^{2+} and Fe^{3+} cations.[14] The peaks generally shift to high binding energy and broaden for Fe_3O_4 due to the appearance of $Fe^{2+}(2p_{3/2})$ and $Fe^{2+}(2p_{1/2})$, while the presence of the satellite peak at around 719.2 eV is characteristic of γ-Fe_2O_3.[15] In our case, the levels of $Fe2p_{3/2}$ and $Fe2p_{1/2}$ are, respectively, 710.7 and 724.4 eV for γ-Fe_2O_3 and α-Fe_2O_3; 711.1 and 724.9 eV for Fe_3O_4, and a satellite peak at 719.2 eV (indicated by the arrow) is observed for γ-Fe_2O_3 and α-Fe_2O_3. In addition, no satellites for Fe_3O_4 can be identified, excluding the presence of γ-Fe_2O_3 or α-Fe_2O_3 in the Fe_3O_4 samples, which is in good agreement with the above literatures [14,15]. The XPS patterns are well in agreement with the XRD data and reveal that complete phase transformation could be achieved by the method used here.

In addition, we also investigated the dispersion properties of the three samples in organic solvent. Although the three samples have a large size, they all can be easily dispersed in the dispersants such as oleic acid and liquid paraffin, while still keeping the stability for a few hours under room temperature, as clearly shown in the insets of panels (a)−(d) of Figures 1. The dispersed Fe_3O_4, γ-Fe_2O_3, and Fe dendritic microstructures can be easily separated from the dispersant by using a magnet, which is characteristic for ferromagnets, but the α-Fe_2O_3 cannot be separated (Figures 1e−g). Moreover, many experiments show that this phase transformation approach for the three dendritic microstructures has excellent reproducibility, and the resulting structures are highly stable, without morphological or compositional change over several months when stored in air.

The representative overview FE-SEM images of the as-synthesized samples are shown in panels (a) of Figures 2, 3, and 4. Compared with that of the precursor α-Fe_2O_3,[4] we can see that on conversion from α-Fe_2O_3 to Fe_3O_4 and γ-Fe_2O_3 not only the dendritic morphology but also the size is perfectly maintained. As shown in panels (b) of Figures 2 and 3, the high-magnification images of a single dentrite, all dendrites have similar structure (a hierarchical structure with tertiary branches), which is the same as the precursor α-Fe_2O_3 micropine dendrites. The lengths of the dendrite trunks are 3−5 μm, and those of the branch trunk range from 50 nm to 1.5 μm. But, by carefully comparing the electron microscopy of a single γ-Fe_2O_3 dendrite with that of Fe_3O_4, it was found that the branch surface of

γ-Fe_2O_3 microdendrites is smoother than that of Fe_3O_4 microdendrites. Further structural characterization for the Fe_3O_4 and γ-Fe_2O_3 dendrites was carried out by SAED and HRTEM (Figure 2c , d, Figure 3c, d). The orderly lattice fringes and the SAED patterns show that the dendritic Fe_3O_4 and γ-Fe_2O_3 dendrites both are single crystalline, indicating that the single-crystal nature is well preserved, and crystallographic orientations are also observed, [110] for Fe_3O_4 and [111] for γ-Fe_2O_3. In addition, the insets of panel (a) of Figure 2amd panel (b) of Figure 3 are schematic diagrams for the partially filled unit cell of Fe_3O_4 and γ-Fe_2O_3 from the direction of [001], which clearly verifies that the as-obtained Fe_3O_4 and γ-Fe_2O_3 microdendrites possess different crystal structures, and the conversion from α-Fe_2O_3 to Fe_3O_4 involves sheaving of the oxide ion planes from AB to ABC stacking, not a topotactic phase change. However, Fe_3O_4 then to γ-Fe_2O_3 is a topotactic phase change.

When the precursor α-Fe_2O_3 micropines were fully reduced under an appropriate temperature, dendritic Fe micropines were still obtained, as shown in panel (a) of Figure 4. The inset of panel (a) of Figure 4 also clearly indicates the crystal structure of Fe from the direction of [001], which confirms the body-centered cubic phase of dendritic Fe micropines. However, from panels (b) and (c) of Figure 4, we found that although the morphology is preserved, there is an evident change in the size and hierarchical structure. The size of the whole dendrite is reduced on conversion from α-Fe_2O_3 to Fe. In addition to this, the perfect hierarchical structure characteristic has completely transformed into a hierarchical structure only with secondary branches. The reason may be that for the conversion from α-Fe_2O_3 to Fe, the final Fe phase must get rid of all oxygen atoms, resulting in a reduced size and shrinkage of the structure. Panels (d)−(g) of Figure 4 show HRTEM images taken in the different areas labeled in panel (c) of Figure 4. It is obvious that all of them show clear lattice fringes, indicating the single-crystalline nature of the whole dendrite. Different areas all have same lattice spacing of 0.203 nm between adjacent lattice planes, corresponding to the distance between two (110) crystal planes. This result indicates that both the stem and branches are oriented along [110] direction. The SAED taken on the same dendrite but at different areas all show the same image as in panel (h) of Figure 4, also confirming the single-crystalline nature of the dendrite.

We know that iron-based materials often have intriguing magnetic properties because of the structure, shape anisotropy, and crystallinity can evidently influence the magnetic properties of microstructured and nanostructured materials, Therefore, we examined the magnetic properties of Fe_3O_4, γ-Fe_2O_3, and Fe dendritic microstructures on a SQUID magnetometer. Panels (a)−(c) of Figure 5 show the magnetic hysteresis loops (M−H loops) combined with the expanded low-field hysteresis curves (insets of Figure 5a−c) of the dendritic crystals measured at 5 and 300 K, which indicate the magnetic properties, including saturation magnetization Ms and the coercivity Hc, respectively. As shown in panel (a) of Figure 5, the magnetic saturation is reached with the external field of about 10 kOe for Fe_3O_4 dendritic microstructures. Panel (a) of Figure 5 also shows that the Ms values of Fe_3O_4 dendritic microstructures are about 101.5 emu/g at 5 K and 95 emu/g at 300 K. The inset of panel (a) of Figure 5 clearly shows the Hc values are about 706.5 Oe at 5 K and 271.4 Oe at 300 K. In general, Ms values for magnetic nanomaterials are lower than those for corresponding bulk materials because the spin disorder on the surface and surface oxidation would significantly reduce the total magnetic moment.

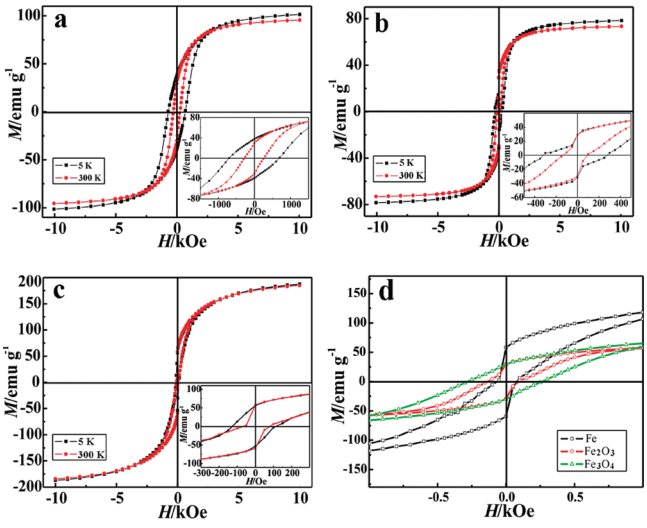

Figure 5. Magnetic hysteresis loops of (a) Fe_3O_4 dendritic microstructures, (b) γ-Fe_2O_3 dendritic microstructures, and (c) Fe dendritic microstructures. Insets of panels (a)−(c) are expanded low field hysteresis curves. (d) Comparison of hysteresis curves of the three samples at 300 K.

But for this instance, the Ms value for Fe_3O_4 dendritic microstructures at 300 K is very close to the value of bulk Fe_3O_4 (Ms = 92 emu/g, 300 K), which may attribute to the high crystallinity of as-prepared dendritic micropines.[5f] However, for the instance of γ-Fe_2O_3 and Fe dendritic microstructures, the Ms value of γ-Fe_2O_3 dendritic microstructures is about 78.9 emu/g for the loop at 5 K and 73.4 emu/g at 300 K, and the Hc value is about 320.5 Oe for the loop at 5 K and 135.7 Oe at 300 K (Figure 5b and the inset). The Ms value of Fe dendritic microstructures is about 187.8 emu/g for the loop at 5K and 183.7 emu/g at 300 K, and the Hc value is about 128.0 Oe for the loop at 5 K and 81.5 Oe at 300 K (Figure 5c and the inset). The Ms values for γ-Fe_2O_3 and Fe dendritic microstructures at 300 K are significantly lower than the values of bulk materials (Ms_{Fe} = 217.6 emu/g; $Ms_{\gamma\text{-}Fe2O3}$ = 76 emu/g, 300 K) and higher than the values of nanoparticles,[16] which are a typical characteristic of ferromagnetic materials and may attribute to the crystallinity and surface defects of as-prepared dendritic micropines via oxidation or complete reduction. In addition, a comparison of the Hc values of Fe_3O_4, γ-Fe_2O_3, and Fe dendritic microstructures is shown in panel (d) of Figure 5. From panel (d) of Figure 5, we can conclude that $Hc_{Fe3O4} > Hc_{\gamma\text{-}Fe2O3} > Hc_{Fe}$, which is a key factor that determines their microwave absorbability described below.[10]

To reveal the microwave absorption properties of the as-synthesized samples, the reflection loss (RL) values of Fe_3O_4, γ-Fe_2O_3, and Fe dendritic microstructures were calculated using the relative complex permeability and permittivity at a given frequency and thickness layer according to the transmit line theory, which is summarized as the following equations[17]

$$Z_{in} = Z_0\sqrt{\mu_r/\varepsilon_r}\tanh\left[j(2\pi fd/c)\sqrt{\mu_r\varepsilon_r}\right] \quad (1)$$

$$\mathrm{RL}(dB) = 20\log\left|(Z_{in}-Z_0)/(Z_{in}+Z_0)\right| \quad (2)$$

where f is the microwave frequency, d is the thickness of the absorber, c is the velocity of light, Z_0 is the impedance of air, and Z_{in} is the input impedance of the absorber. The relative complex permeability and permittivity were tested on a network analyzer

dx.doi.org/10.1021/cm103441u |Chem. Mater. 2011, 23, 1587–1593

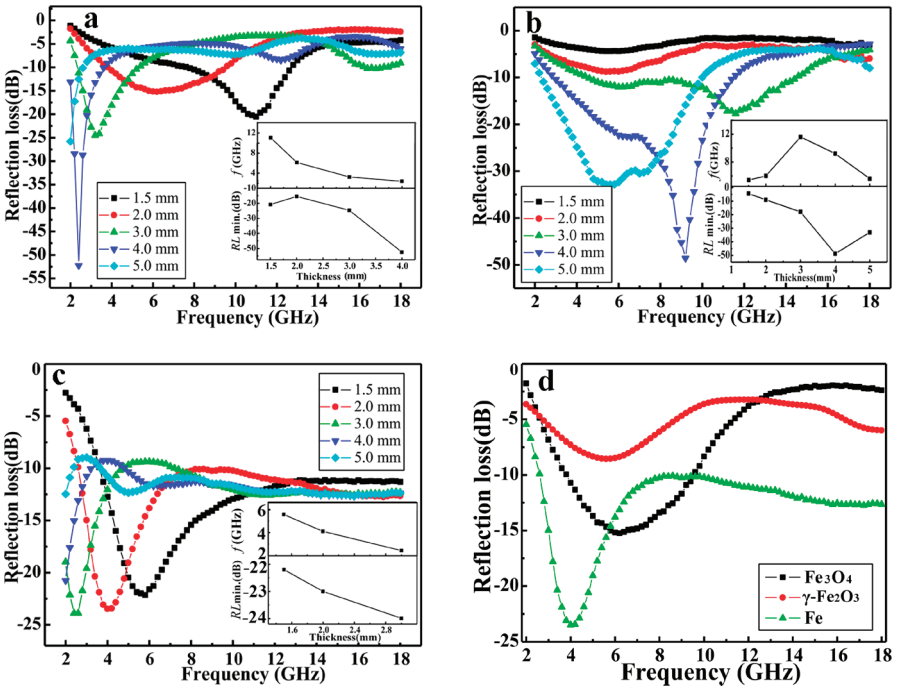

Figure 6. Microwave reflection losses of (a) Fe_3O_4 dendritic microstructures, (b) γ-Fe_2O_3 dendritic microstructures, and (c) Fe dendritic microstructures/paraffin wax composites versus frequency. (d) Comparison of microwave reflection losses of the three samples with the thickness of 2 mm. Insets of panels (a)−(c) are graphs of the dependence of the RL minimum and the corresponding frequency upon the sample thickness.

with the frequency of a 2−18 GHz range. The thickness of the sample is one of the crucial parameters that affects the intensity and the position of the frequency at the RL minimum. Therefore, we prepared these three samples with the same thickness of 1.5, 2, 3, 4, and 5 mm in order to eliminate the influence resulting from the thickness of the samples. The results are shown in Figure 6. As shown in Figure 6, we find that the three samples exhibit excellent microwave absorption properties. For Fe_3O_4 dendritic microstructures, there is only one sharp and strong peak at 2.2 GHz with the minimum RL of −53.0 dB when the thickness of the Fe_3O_4 sample is 4 mm, and two broad peaks (3.3 GHz, 24.6 dB and 16.6 GHz, −10.4 dB) were observed with the thickness of 3 mm (Figure 6a). For Fe_3O_4 dendritic microstructures, the minimum RL is −53.0 dB with the sample thickness of 4 mm, which is better than those in the previous reports: Fe_3O_4 microspheres with a size of 750 nm (−45.2 dB, 4 mm),[18a] Fe_3O_4 nanospheres with sizes of about 300 nm (−30.3 dB, 5.5 mm),[11b] and Fe_3O_4 nanoparticles with the sizes of about 50−100 nm (−35.0 dB, 4.41 mm).[18b] Whereas for γ-Fe_2O_3 dendritic microstructures, there is one broad and strong wave absorbing peak in the range of 2−13 GHz, and the minimum RL even reaches −50.0 dB with the thickness of 4 mm, and a broad peak (2−13 GHz, −33.2 dB) with the thickness of 4 mm was observed (Figure 6b). So far, to the best of our knowledge, there is no related report on the microwave absorption properties of γ-Fe_2O_3. As shown in panel (c) of Figure 6, for Fe dendritic microstructures, the peak intensity and frequency both decrease when the thickness increases, and the minimum RL reaches −25.0 dB with the frequency of 2.5 GHz when the thickness is 3 mm. According to this trend, stronger absorbing peaks for the sample thickness of 4 or 5 mm are expected for the long-wavelength or low-frequency regime, i.e., 0.1−2 GHz. However, because of the limited equipment, we cannot show them here. The experimental results show that the thickness of the Fe dendritic-microstructured sample is about 1.5 mm, and the minimum RL is −22.5 dB, which is thinner than those in other report on Fe nanoflakes coating with SiO_2 nanoshell (−22.5 dB, 2.5 mm).[11a] Furthermore, a study by Peng and co-workers has shown that a pure Fe sheet exhibits hardly any microwave absorption because of its low electric resistivity and strong skin effect at high frequency.[19] It is known that the absorption properties of a material are closely related to the structures of absorbents.[7b,20] The assembly of the magnetic nanostructures into well-defined hierarchical microstructures is believed to increase the geometrical effect when an electromagnetic wave is radiated on these materials, leading to enhanced absorption abilities. Therefore, hierarchical microstructures may be appealing in improving the electromagnetic wave absorptions. In our case, the excellent microwave absorption properties of Fe-based compound dendritic microstructures may be ascribed to the hierarchical dendrite-like structures and the nanometer size of the branch. However, the difference of the microwave absorbability of these microstructured materials is attributed to their different coercivity.[10] The insets in panels (a)−(c) of Figure 6 are the graph of the dependence of the RL minimum and the corresponding frequency upon the sample thickness, from which it was found that only Fe dendritic microstructures present the decreasing rule, i.e., the peak intensity and the corresponding frequency for a Fe sample increase with the decrease in thickness (inset in Figure 6c). But for Fe_3O_4 dendritic microstructures, the minimum of RL first increases and then decreases with the decrease in thickness, and for γ-Fe_2O_3 dendritic microstructures, the opposite situation occurs. The corresponding frequency shows a single increase for Fe_3O_4 dendritic microstructures, and first an increase and then a decrease for γ-Fe_2O_3 dendritic microstructures when the thickness decreases (insets in Figures 6a and b). Panel (d) of Figure 6 shows a comparison of the microwave RL of the three samples with the same

dx.doi.org/10.1021/cm103441u |*Chem. Mater.* 2011, 23, 1587–1593

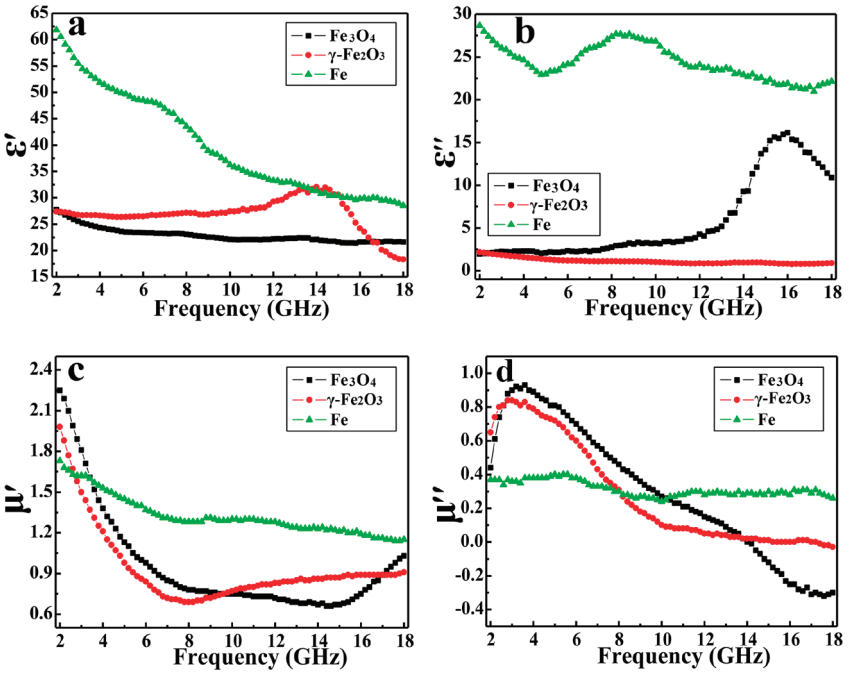

Figure 7. Frequency dependence of (a) real and (b) imaginary parts of complex permittivity and (c) real and (d) imaginary parts of complex permeability for Fe_3O_4, γ-Fe_2O_3 and Fe dendritic microstructures.

thickness of 2 mm. As illustrated in panel (d) of Figure 6, the RL minimums reach −25.0, −15.2, and −8.7 dB with the frequency of 4.0, 6.1, and 5.7 GHz for Fe, γ-Fe_2O_3, and Fe_3O_4 dendritic microstructures, respectively.

To investigate the possible mechanism of microwave absorption of the above three samples, we independently measured the complex relative permittivity and permeability of the samples. Figure 7 shows the real and imaginary parts of the complex relative permittivity (ε', ε'') and permeability (μ', μ'') measured for the three samples. Electronic spin and charge polarization due to point effect and polarized centers may also have a profound effect on the response of Fe_3O_4 dendritic microstructures.[17] For Fe_3O_4 dendritic microstructures, the ε' value negligibly decreases with increasing frequency from 27.9 to 21.6 in the 2−18 GHz range, and the ε'' value exhibits a strong peak in the 12−18 GHz range (Figure 7a, b), indicating a resonance behavior, which is expected when the sample is highly conductive and the skin effect becomes significant. Moreover, the μ' value obviously decreases with increasing frequency from 2.3 to 0.6 in the 2−14.6 GHz range and then increases to 1.0, and the ε'' value exhibits a strong peak at 4 GHz (Figure 7c, d), which is attributed to the larger *Hc* values of the Fe_3O_4 dendritic microstructures (Figure 5d).[10] The similar analysis can be used for γ-Fe_2O_3 dendritic microstructures. But for Fe dendritic microstructures, the ε' value sharply decreases with increasing frequency from 62.5 to 28.5 in the 2−18 GHz range, and the ε'' value exhibits a complex variation in the 12−18 GHz range and shows a peak in the 4.9−11.7 GHz range (Figure 7a, b). But the variation both μ' and μ'' are negligibly small (Figure 7c, d), indicating almost no magnetic loss contribution from the sample to the microwave absorption, which is agreement with the smaller *Hc* value of Fe dendritic microstructures (Figure 5d). As we know, there are two possible contributions for microwave absorption: dielectric loss and magnetic loss. It is well-known that the permittivity and permeability are mainly originated from electronic polarization, ion polarization, intrinsic electric dipole polarization, and their magnetic properties,[7b,21] on which the crystal structure, size, and special geometrical morphology may have an important influence. Therefore, in our case, Fe sample is the electrical loss rather than magnetic loss material. Whereas, microwave absorption properties of Fe_3O_4 and γ-Fe_2O_3 dendritic microstructures may be ascribed to their dielectric loss and excellent magnetic loss properties. By combining the above magnetic data (Figure 5d) with the discussion on the influence of ε', ε'', μ', and μ'', the reason that the three samples studied here have different microwave absorption properties can be clearly explained.

CONCLUSIONS

In conclusion, a facile method has been successfully developed for the synthesis of Fe_3O_4, γ-Fe_2O_3 ,and Fe micropine dendrites with single-crystal structure via reduction or oxidation of α-Fe_2O_3 obtained by hydrothermal reaction of $K_3[Fe(CN)_6]$ in aqueous solution. The magnetic properties and microwave absorbability of the hierarchical dendritic microstructures have been investigated carefully. Magnetism and microwave absorption analysis indicate that the dendrites are typically characteristic of ferromagnetic materials and exhibit excellent microwave absorbability in low or middle frequency (2−9 GHz). This represents a new platform for further studies of microstructured or nanostructured materials for application as microwave-absorbing materials.

ASSOCIATED CONTENT

Supporting Information. Complete information for ref 15b. This material is available free of charge via the Internet at http://pubs.acs.org.

AUTHOR INFORMATION

Corresponding Author

*E-mail: gbsun@bnu.edu.cn (G.S.); caomh@bit.edu.cn (M.C.); weib@UDel.Edu (B.W.); Tel: +86-10-62242577; Fax: +86-10-58802750.

ACKNOWLEDGMENT

This work was supported by the Natural Science Foundation of China (NSFC, 20901010, 20731002, 20871016, 91022006, and 20973023) and Program for New Century Excellent Talents in University. Prof. Wei B. Q. is thankful for the support of the 111 Project (B07012).

REFERENCES

(1) (a) Dinsmore, A.; Hsu, M.; Nikolaides, M.; Marquez, M.; Bausch, A.; Weitz, D. *Science* **2002**, *298*, 1006. (b) Bigi, A.; Boanini, E.; Walsh, D.; Mann, S. *Angew. Chem., Int. Ed.* **2002**, *41*, 2163. (c) Yuan, J.; Laubernds, K.; Zhang, Q.; Suib, S. *J. Am. Chem. Soc.* **2003**, *125*, 4966. (d) Liu, B.; Zeng, H. *J. Am. Chem. Soc.* **2004**, *126*, 8124. (e) Sukhanova, A.; Baranov, A.; Perova, T.; Cohen, J.; Nabiev, I. *Angew. Chem., Int. Ed.* **2006**, *45*, 2048.

(2) (a) Whetten, R.; Khoury, J.; Alvarez, M.; Murthy, S.; Vezmar, I.; Wang, Z.; Cleveland, C.; Luedtke, W.; Landman, U. *Adv. Mater.* **1996**, *8*, 428. (b) Sun, S.; Murray, C.; Weller, D.; Folks, L.; Moser, A. *Science* **2000**, *287*, 1989. (d) Weiss, P. *ACS Nano* **2008**, *2*, 1085.

(3) Galenko, P.; Zhuravlev, V. *Physics of Dendrites: Computational Experiments*; World Scientific: Singapore, 1994.

(4) Cao, M.; Liu, T.; Gao, S.; Sun, G.; Wu, X.; Hu, C.; Wang, Z. *Angew. Chem., Int. Ed.* **2005**, *44*, 4197.

(5) (a) Lu, L.; Kobayashi, A.; Kikkawa, Y.; Tawa, K.; Ozaki, Y. *J. Phys. Chem. B* **2006**, *110*, 23234. (b) Fang, J.; You, H.; Kong, P.; Yi, Y.; Song, X.; Ding, B. *Cryst. Growth Des.* **2007**, *7*, 864. (c) Fan, L.; Guo, R. *Cryst. Growth Des.* **2008**, *8*, 2150. (d) Yan, C.; Xue, D. *Cryst. Growth Des.* **2008**, *8*, 1849. (e) Zhu, L.; Xiao, H.; Zhang, W.; Yang, Y.; Fu, S. *Cryst. Growth Des.* **2008**, *8*, 1113. (f) Ye, J.; Chen, Q.; Qi, H.; Tao, N. *Cryst. Growth Des.* **2008**, *8*, 2464.

(6) Qiu, R.; Zhang, X.; Qiao, R.; Li, Y.; Kim, Y.; Kang, Y. *Chem. Mater.* **2007**, *19*, 4174.

(7) (a) Li, G.; Lu, X.; Qu, D.; Yao, C.; Zheng, F.; Bu, Q.; Dawa, C.; Tong, Y. *J. Phys. Chem. C* **2007**, *111*, 6678. (b) Zhuo, R.; Feng, H.; Chen, J.; Yan, D.; Feng, J.; Li, H.; Geng, B.; Cheng, S.; Xu, X.; Yan, P. *J. Phys. Chem. C* **2008**, *112*, 11767. (c) Chen, D.; Ye, J. *Adv. Funct. Mater.* **2008**, *18*, 1922. (d) Wang, Q.; Xu, G.; Han, G. *Cryst. Growth Des.* **2006**, *6*, 1776. (e) Li, D.; Zheng, Z.; Shui, Z.; Long, M.; Yu, J.; Wong, K.; Yang, L.; Zhang, L.; Lau, W. *J. Phys. Chem. C* **2008**, *112*, 2845. (f) Li, G.; Yao, C.; Lu, X.; Zheng, F.; Feng, Z.; Yu, X.; Su, C.; Tong, Y. *Chem. Mater.* **2008**, *20*, 3306.

(8) Purkayastha, A.; Yan, Q.; Raghuveer, M.; Gandhi, D.; Li, H.; Liu, Z.; Ramanujan, R.; Borca-Tasciuc, T.; Ramanath, G. *Adv. Mater.* **2008**, *20*, 2679.

(9) (a) Zitoun, D.; Respaud, M.; Fromen, M.; Casanove, M.; Lecante, P.; Amiens, C.; Chaudret, B. *Phys. Rev. Lett.* **2002**, *89*, 37203. (b) Wen, X.; Wang, S.; Ding, Y.; Wang, Z.; Yang, S. *J. Phys. Chem. B* **2005**, *109*, 215. (c) Shevchenko, E.; Talapin, D.; Schnablegger, H.; Kornowski, A.; Festin, O.; Svedlindh, P.; Haase, M.; Weller, H. *J. Am. Chem. Soc.* **2003**, *125*, 9090. (d) Guo, L.; Liang, F.; Wang, N.; Kong, D.; Wang, S.; He, L.; Chen, C.; Meng, X.; Wu, Z. *Chem. Mater.* **2008**, *20*, 5163. (e) Wang, N.; Cao, X.; Kong, D.; Chen, W.; Guo, L.; Chen, C. *J. Phys. Chem. C* **2008**, *112*, 6613.

(10) Ohkoshi, S.; Kuroki, S.; Sakurai, S.; Matsumoto, K.; Sato, K.; Sasaki, S. *Angew. Chem., Int. Ed.* **2007**, *46*, 8392.

(11) (a) Yan, L.; Wang, J.; Han, X.; Ren, Y.; Liu, Q.; Li, F. *Nanotechnology* **2010**, *21*, 095708. (b) Jia, K.; Zhao, R.; Zhong, J.; Liu, X. *J. Magn. Magn. Mater.* **2010**, *332*, 2167. (c) Tuček, J.; Zbořil, R.; Namai, A.; Ohkoshi, S. *Chem. Mater.* **2010**, *22*, 6483. (d) Namai, A.; Sakurai, S.; Nakajima, M.; Suemoto, T.; Matsumoto, K.; Goto, M.; Sasaki, S.; Ohkoshi, S. *J. Am. Chem. Soc.* **2009**, *131*, 1170.

(12) (a) Dumestre, F.; Chaudret, B.; Amiens, C.; Renaud, P.; Fejes, P. *Science* **2004**, *303*, 821. (b) Dyal, A.; Loos, K.; Noto, M.; Chang, S.; Spagnoli, C.; Shafi, K.; Ulman, A.; Cowman, M.; Gross, R. *J. Am. Chem. Soc.* **2003**, *125*, 1684. (c) Zeng, H.; Li, J.; Liu, J.; Wang, Z.; Sun, S. *Nature* **2002**, *420*, 395. (d) Yavuz, C.; Mayo, J.; Yu, W.; Prakash, A.; Falkner, J.; Yean, S.; Cong, L.; Shipley, H.; Kan, A.; Tomson, M.; Natelson, D.; Colvin1, V. *Science* **2006**, *314*, 964. (e) Chueh, Y.; Lai, M.; Liang, J.; Chou, L.; Wang, Z. *Adv. Funct. Mater.* **2006**, *16*, 2243.

(13) Brezesinski, T.; Groenewolt, M.; Antonietti, M.; Smarsly, B. *Angew. Chem., Int. Ed.* **2006**, *45*, 781.

(14) (a) Cornell, R.; Schwertmann, U. *The Iron Oxides: Structure, Properties, Reactions, Occurrence and Uses*; VCH, Weinheim, New York, 1996. (b) Fujii, T.; de Groot, F.; Sawatzky, G.; Voogt, F.; Hibma, T.; Okada, K. *Phys. Rev. B* **1999**, *59*, 3195.

(15) (a) Teng, X.; Black, D.; Watkins, N.; Gao, Y.; Yang, H. *Nano Lett.* **2003**, *3*, 261. (b) Jia, C.; et al. *J. Am. Chem. Soc.* **2008**, *130*, 16968.

(16) (a) Lai, J.; Shafi, K.; Ulman, A.; Loos, K.; Popovitz-Biro, R.; Lee, Y.; Vogt, T.; Estournés, C. *J. Am. Chem. Soc.* **2005**, *127*, 5730. (b) Latham, A.; Wilson, M.; Schiffer, P.; Williams, M. *J. Am. Chem. Soc.* **2006**, *128*, 12632.

(17) (a) Matsumoto, M.; Miyata, Y. *IEEE Trans. Magn.* **1997**, *33*, 4459. (b) Singh, P.; Babbar, V.; Razdan, A.; Puri, R.; Goel, T. *J. Appl. Phys.* **2000**, *87*, 4362. (c) Maeda, T.; Sugimoto, S.; Kagotani, T. *J. Magn. Magn. Mater.* **2004**, *284*, 113. (d) Han, X.; Wang, Y. *Phys. Scr.* **2007**, *T129*, 335.

(18) (a) Ni, S.; Sun, X.; Wang, X.; Zhou, G.; Yang, F.; Wang, J.; He, D. *Mater. Chem. Phys.* **2010**, *124*, 353. (b) Qiang, C.; Xu, J.; Zhang, Z.; Tian, L.; Xiao, S.; Liu, Y.; Xu, P. *J. Alloys Compd.* **2010**, *506*, 93.

(19) Che, R.; Peng, L.; Duan, X.; Chen, Q.; Liang, X. *Adv. Mater.* **2004**, *16*, 401.

(20) (a) Li, H.; Huang, Y.; Sun, G.; Yan, X.; Yang, Y.; Wang, J.; Zhang, Y. *J. Phys. Chem. C* **2010**, *114*, 10088. (b) Zhao, H.; Zhang, B.; Zhang, J.; Zhang, L.; Han, X.; Xu, P.; Zhou, Y. *J. Phys. Chem. C* **2010**, *114*, 21214. (c) Qi, X.; Deng, Y.; Zhong, W.; Yang, Y.; Qin, C.; Au, C.; Du, Y. *J. Phys. Chem. C* **2010**, *114*, 808.

(21) (a) Wen, H.; Cao, M.; Sun, G.; Xu, W.; Wang, D.; Zhang, X.; Hu, C. *J. Phys. Chem. C* **2008**, *112*, 15948. (b) Sun, G.; Zhang, X.; Cao, M.; Wei, B.; Hu, C. *J. Phys. Chem. C* **2009**, *113*, 6948.